SSCL-364

Superconducting Super Collider Laboratory

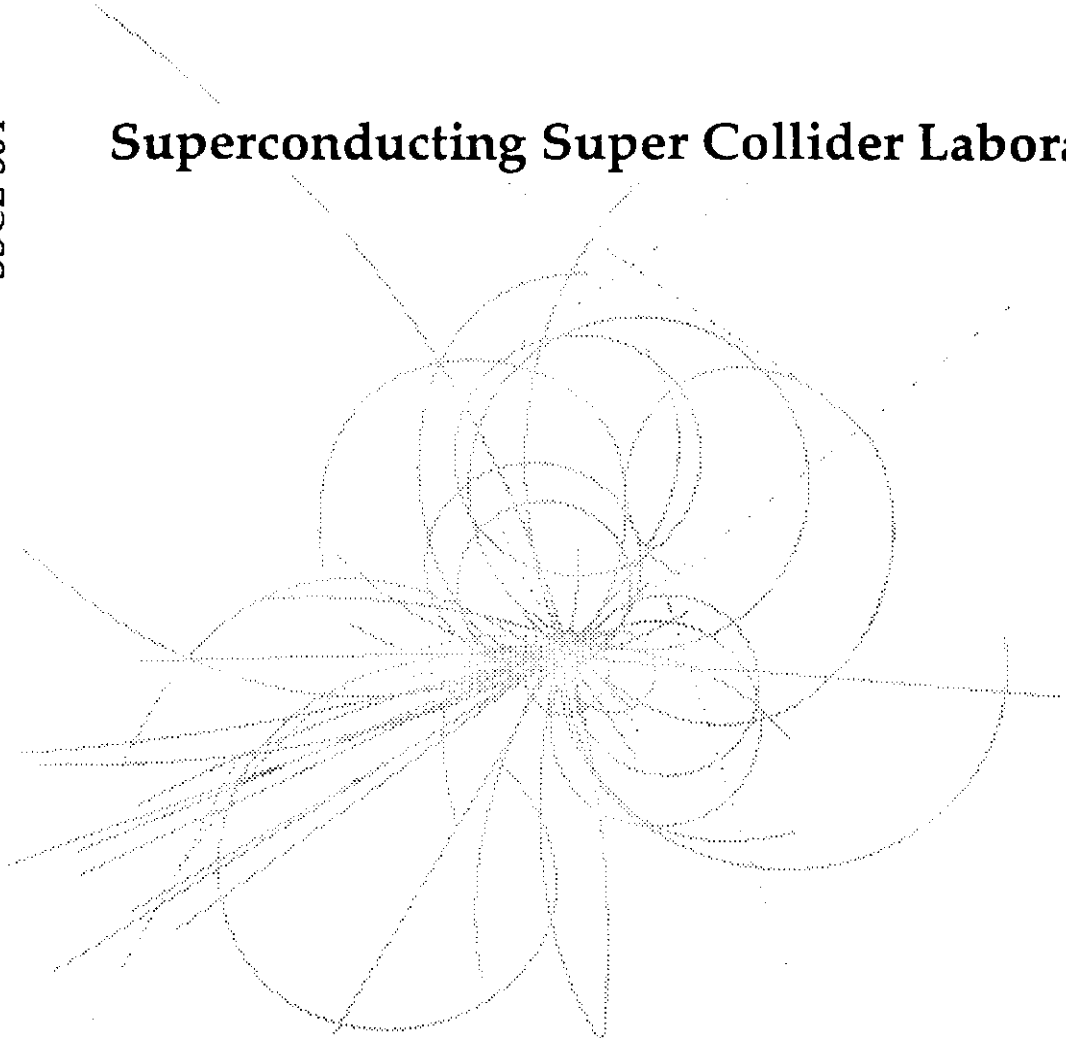

Status of 4-cm-Aperture, 17-m-Long SSC Dipole Magnet R&D Program at BNL Part I: Magnet Assembly

A. Devred, T. Bush, R. Coombes, et al.

March 1991

SSCL-364
FERMILAB Conf 91/322
LBL-31038

STATUS OF 4-CM-APERTURE, 17-M-LONG SSC DIPOLE MAGNET R&D PROGRAM AT BNL PART I: MAGNET ASSEMBLY*

A. Devred, T. Bush, R. Coombes, J. DiMarco, C. Goodzeit, J. Kuzminski, M. Puglisi, P. Radusewicz, P. Sanger, R. Schermer, J. Tompkins, J. Turner, Z. Wolf, Y. Yu, and H. Zheng

Magnet Division
Superconducting Super Collider Laboratory†
2550 Beckleymeade Avenue
Dallas, TX 75237 USA

T. Ogitsu

Superconducting Super Collider Laboratory and
KEK, National Laboratory for High Energy Physics
1-1 Oho, Tsukuba-shi
Ibaraki-ken 305 Japan

M. Anerella, J. Cottingham, G. Ganetis, M. Garber, A. Ghosh, A. Greene, R Gupta, J. Herrera, S. Kahn, E. Kelly, A. Meade, G. Morgan, J. Muratore, A. Prodell, M. Rehak, E. P. Rohrer, W Sampson, R. Shutt, P. Thompson, P. Wanderer, and E. Willen

Brookhaven National Laboratory
Upton, NY 11973 USA

M. Bleadon, R. Hanft, M. Kuchnir, P. Mantsch, P. O. Mazur, D. Orris, T. Peterson, and J. Strait

Fermi National Accelerator Laboratory
P.O. Box 500
Batavia, IL 60510 USA

J. Royet, R. Scanlan, and C. Taylor

Lawrence Berkeley Laboratory
Berkeley, CA 94720 USA

*Presented at the Third International Industrialization Symposium on the Super Collider (IISSC), Atlanta, Georgia, March 13–15, 1991.
†Operated by the Universities Research Association, Inc., for the U.S. Department of Energy, under Contract No. DE-AC02-89ER40486.

Abstract: Over the last year, several 4-cm-aperture, 17-m-long dipole magnet prototypes were built by Brookhaven National Laboratory (BNL) under contract with the Superconducting Super Collider (SSC) Laboratory. These prototypes are the last phase of a half-decade-long R&D program, carried out in collaboration with Fermi National Accelerator Laboratory and Lawrence Berkeley Laboratory, and aimed at demonstrating the feasibility of the SSC main ring magnets. They also lay the ground for the 5-cm aperture dipole magnet program to be started soon. After reviewing the design features of the BNL 4-cm-aperture, 17-m-long dipole magnets, we describe in detail the various steps of their fabrication. For each step, we discuss the parameters that need to be mastered, and we compare the values that were achieved for the five most recent prototypes. The data appear coherent and reproducible, demonstrating that the assembly process is under control.

INTRODUCTION

The key event for the SSC collider dipole magnets during 1990 was the decision taken in January to increase the aperture from 4 cm[1] to 5 cm.[2] The main reason for this decision was to improve the field quality in order to reduce the risk of beam losses.[3] However, the implementation of such a change required the development of new tooling, which would take 12–18 months. It was therefore decided to continue the production of 4 cm aperture prototypes so that design concepts developed for the 4 cm program could be tested before they were scaled up to the 5-cm program.

In this paper, we report on the design and fabrication of the five most recent 4- cm-aperture, 17-m-long collider dipole magnet prototypes. The five cold masses were built at Brookhaven National Laboratory (BNL). Three of them (designated DD0026, DD0027, and DD0028) were cold-tested at Fermi National Accelerator Laboratory (FNAL);[4,5] the two others (designated DC0201 and DC0204) were cold-tested at BNL. In the first part, we shall review the design features of these magnets and try to explain the role of the various components and how they are supposed to interact. In the second part, we shall describe how these components are put together and which parameters need to be controlled during assembly in order to realize the design concepts. All along, we shall summarize the assembly data of the five magnets and discuss their reproducibility and conformity to the design. The cold-test results of these magnets will be presented elsewhere.[6] Also, since the primary focus of these magnets is quench performance rather than field quality, we shall limit our analyses to the mechanical data; we shall not discuss magnetic measurements.

MAGNET FEATURES

Baseline Design

Concepts

The five magnets presented here, like their predecessors, follow the 1986 conceptual design[1] with a 4 cm aperture and a magnetic length of 16.6 m. A cross-sectional view of the cold mass assembly is shown in Figure 1. The dipole field is produced by a two-layer cosine-theta coil that is mechanically constrained, both radially and axially, by stainless-steel collar laminations and stainless-steel end plates. Iron yoke laminations, located outside the collars, enhance the magnetic field by roughly 20 percent. The cold mass is completed by a stainless-steel shell that delimits the region of circulation for the 4.35 K, 0.4 MPa forced flow of supercritical helium. The design current is 6500 A, corresponding to a central field of 6.6 T.

The first full-length collider dipole prototypes that were built (1986-87) exhibited excessive training.[7-9] In order to understand this training behavior, subsequent magnets were

instrumented with voltage taps on the coil inner layer (to locate the quench origins),[10] and with beam-type strain-gauge transducers (to measure the azimuthal pressure exerted by the coil against the collar pole).[11] Strain gauges were also mounted on the external surface of the cold mass shell to measure both radial and azimuthal stresses. Several features of the magnet design were then varied to determine their influence on quench performance. In 1988, it was found that the best performing magnets were those with rigid support of the coil ends against the end plates, and those where the iron yoke contributed to the radial support of the coil by interfering with the collars.[12-14] The design of the collars and the yoke was then modified to ensure that this interference would occur, leading to the concept of *line-to-line fit*, the details of which were refined throughout 1989,[15] and which is now the baseline of the SSC collider dipole program.

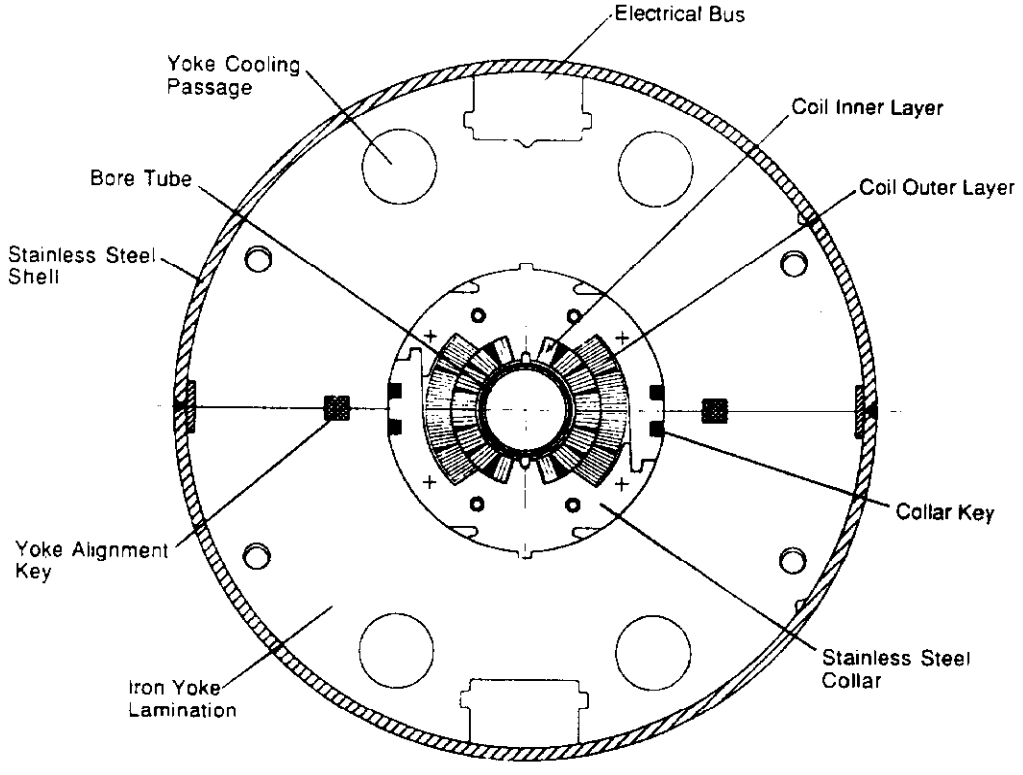

Figure 1. Cross sectional view of the cold mass of BNL 4-cm aperture, 17-m-long collider dipole prototype (DC series).

The starting point of the line-to-line fit design is the decision to make the outer radius of the stainless-steel collar laminations the same as the inner radius of the iron yoke laminations at room temperature. During collaring, the coil is squeezed into the collars with a large azimuthal pre-compression. After collaring, the coil exerts a large pressure against the collar poles, and the collared-coil assembly deflects along the vertical axis, becoming larger than the iron yoke. When the yoke is put on, a gap thus remains between its two halves. This gap is progressively closed during the welding of the outer shell, which is put under tension and compresses the yoke. At the end of welding, the gap is entirely closed, and the outer circumference of the collar and the inner circumference of the yoke fit perfectly. During cool down, the coil shrinks more than the stainless-steel collars, which in turn shrink more than

the iron yoke. The pressure exerted by the coil on the collar poles thus decreases, but it remains large enough to keep deflecting the collars so as to maintain contact with the yoke on the vertical diameter. During excitation, azimuthal stress is redistributed while the coil tends to expand radially, especially at the midplane. The collared-coil assembly thus deflects along the horizontal axis and eventually contacts the yoke. At high currents, the collared-coil assembly thus contacts the yoke along the entire circumference, and the yoke provides a quasi-infinite stiff support against the radial component of the Lorentz force. Also, the yoke defines a clear circular boundary for the collared-coil assembly which is needed to ensure good field quality. At all times, the gap at the midplane of the yoke remains closed due to the compression exerted by the outer shell.

Having briefly explained the concepts underlying the design of these magnets, we shall now review the different components that constitute the cold mass.

Coil

The inner layer of the coil contains 16 turns and 3 copper wedges. It is wound from a 1.6° keystone-angle cable of 23 strands (strand diameter 0.808 mm). The outer layer contains 20 turns and 1 copper wedge and is wound from a 1.2° keystone-angle cable of 30 strands (strand diameter 0.648 mm). The twist pitch of the inner layer conductor is 78.7 mm; that of the outer layer conductor is 73.7 mm. The insulation for both inner and outer cables consists of a layer of 25.4 μm Kapton wrapped with a 50% overlap, completed by a layer of epoxy-impregnated fiberglass wrapped with a 50.8 μm gap. The asymmetric copper wedges serve two purposes: 1) they allow fine tuning of the magnetic field's high-order multipole components, and 2) they allow the coil to assume the correct arch-shape by compensating for the keystone-angle of the cables (which is too small).

Collars

The stainless-steel collar laminations are 1.5 mm thick and 15 mm wide. They are spot-welded in pairs in two configurations, called left and right, and the left and right pairs are stacked together alternately into 149.1-mm-long packs. The spot welding was introduced to increase the rigidity of the collars; the left-right stacking was introduced to eliminate twist in the collared-coil assembly. The collar packs are held together by means of four stainless-steel tubes located near the collar top. They are locked around the coil by four phosphor-bronze tapered keys (3° taper per side, thus 6° total), which are driven horizontally into the keyways located near the midplane. The tapered keys were preferred to the square keys used on earlier prototypes because they limit the peak pressure on the coil during insertion.[16] (Note also that there is a 50 μm clearance between the key and keyway widths; but this has no real significance.)

As we described earlier, the collared coil must be assembled so that, at liquid helium temperature and while energized, the coil remains in azimuthal compression and exerts enough pressure against the collar to ensure vertical contact with the yoke. In other words, the pre-compression of the coil at room temperature must be large enough to compensate for the differences in thermal shrinkage of the various materials during cool down and for the redistribution of azimuthal stress caused by the Lorentz force during energization. On the other hand, the pre-compression should not be too great, for fear of degrading the Kapton insulation and creating a risk of turn-to-turn or coil-to-ground shorts. (Kapton flows easily: it elongates by 3% at room temperature under a pressure of 69 MPa.) A compromise must therefore be reached; a suitable collaring scheme should limit the peak pressure seen by the coil, even while providing enough pre-compression to compensate for the aforementioned losses.

Yoke and Shell

The iron yoke laminations are 1.5 mm thick and 77.47 mm wide. They are compactly stacked into 146.4-mm-long modules, held together by stainless-steel tubes. The yoke modules are assembled around the collared coil so that the split between the two halves is located at the midplane (see Figure 1). The modules are separated by two 1.5-mm-thick stainless-steel laminations, which are slotted for helium venting (see below, "Cross-Flow Cooling"). The two identical keys at the yoke midplane serve two purposes: 1) precise alignment of the yoke modules, and 2) correction of the iron saturation effects on the magnetic field. To avoid over-constraining the alignment, only one key is used for registration, while the other is set loose by oversizing its keyway by about 125 μm. (The side of the laminations with the correctly sized keyway is marked by a notch on the outer perimeter.) The correction of the iron saturation effects will be described in a later paragraph (see below, "Revised Yoke and Yoke Alignment Key"). The outer stainless-steel shell is 4.77 mm thick and consists of two halves welded around the yoke. The welds are also located at the yoke midplane.

As described earlier, in order to create sufficient interference between the collared-coil assembly and the yoke, the assembly's vertical diameter is allowed to become larger than the yoke's. Immediately after inserting the collared coil in the yoke, a gap remains between the yoke halves. It is important, however, that this gap close during the welding of the shell, because if it were to remain open in the cold state, it would alter the rigidity of the yoke where the radial component of the Lorentz force is the largest and would distort the magnetic field. (The field distortion was calculated to be significant only if the gap is larger than 250 μm.) This implies that the vertical deflection of the collared-coil assembly must be kept within reasonable limits.

End Parts

Figure 2 presents a cut-away view of magnet DD0027 end parts. The coil ends maintain the same radial dimension as the straight sections. The spacing of the turns is determined to minimize the harmonic content of the ends. The main spacers are made of laminated, epoxy-impregnated fiberglass. Additional G10 spacers are also inserted between some of the turns to enforce the turn-to-turn insulation. These spacers were determined empirically to position the conductors in an approximate constant perimeter configuration. The axial motion of each end of the coil is restrained by a G10 shoe. This shoe is pressed on by four screws set in the 35-mm-thick stainless-steel end plates. The end plates themselves are anchored to a stainless-steel ring, called the *bonnet*, which is in turn welded to the outer shell. In order to decrease the magnetic field on the end turns, the iron yoke laminations are terminated 47.2 mm before the end of the outer coil straight section, and the last two yoke modules over the coil ends are made of non-magnetic stainless-steel laminations. These laminations are bonded with epoxy to keep the yoke laminations perpendicular to the magnet axis and avoid "angling" during the skinning process, or if there is movement of the end collars due to axial extension of the coil from the Lorentz forces.

Variants

Having briefly presented the common features of these magnets, we shall now review their differences, which are summarized in Table 1.

Copper-to-Superconductor Ratio

All these magnets have a nominal copper-to-superconductor ratio of 1.5 to 1, except DC0204, for which the ratio is 1.29 to 1. The lower ratio was employed in order to pursue the possibility, suggested by short sample tests, that copper-to-superconductor ratio could

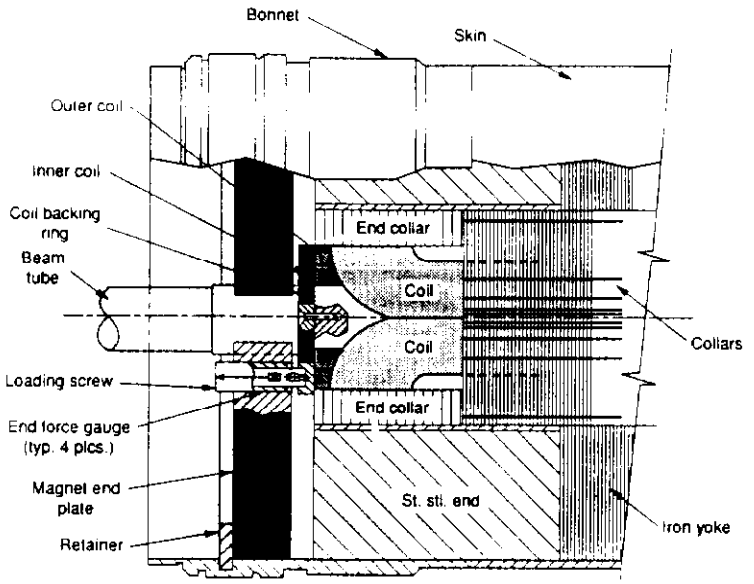

Figure 2. Cut away view of the non-lead end part of BNL 4-cm aperture, 17-m-long collider dipole prototype.

play a significant role in training performance.[17] (Of the four forthcoming DC series magnets, two will employ the lower and two the higher ratio in order to adjudicate this issue.)

Epoxy Content of Inner Layer Conductor Fiberglass Wrap

After magnet DC0201, the epoxy content of the fiberglass wrap around the inner layer conductor was decreased from 24% to 20% in weight in order to curtail epoxy buildup on the inner surface of the coils.

Collar Material: Nitronic-40 versus High Manganese Steel

All magnets use Nitronic 40, 90 kpsi collars, except DD0026, which uses High Manganese steel developed by Kawasaki Steel Corporation. This steel was tried because its integrated thermal shrinkage between 300 K and 4.2 K is lower than that of Nitronic 40, 1.7×10^{-3} compared to 3.0×10^{-3}, and is thus slightly less than that of the yoke, 2.0×10^{-3}. This would seem to allow more even contact of the yoke and the collared coil assembly during cool down. On the other hand, the loss of coil pre-stress with the High Manganese steel collars can be expected to be greater

Collar Shape: Round versus Anti-Ovalized

Magnets up to and including DD0028 used *round* collars. The deflection of the collared coil assembly, however, which was measured to be about 250 μm on the vertical diameter, was deemed excessive and thought to contribute to potential gaps between the yoke halves. Magnets following DD0028, therefore, employed *anti-ovalized* collars, intended to compensate for this deflection. The main difference between the round and anti-ovalized collars resides in the location of the keyways with respect to the midplane, as detailed in Figure 3. In the round collars, the keyways are placed so that when the top and bottom collars are joined and keyed (with no coil in them), their centers coincide, resulting in a round shape. In the anti-ovalized collars, the location of the keyways has been modified so that when joined and keyed, the centers of the top and bottom collars are shifted by 254 μm, reducing the collars' vertical diameter by the same amount. (The anti-ovalized collar keyways are also closer to the midplane to enhance the collar rigidity in this area.)

Table 1. Variants in Design Features of Most Recent BNL 4-cm Aperture, 17-m-Long Collider Dipole Prototypes.

	DD0026	DD0027	DD0028	DC0201	DC0204
Inner Conductor Copper-to-Superconductor Ratio	1.44	1.48	1.52	1.52	1.29
Inner Conductor Critical Current at 4.22K and 7T*	7465 A	7822 A	7893 A	7893 A	8368 A
Epoxy Content of Inner Conductor Fiberglass Wrap	24%	24%	24%	24%	20%
Collar Material	High Manganese	Nitronic 40	Nitronic 40	Nitronic 40	Nitronic 40
Collar Shape	Round	Round	Round	Anti-Ovalized	Anti-Ovalized
Collar-Yoke Shim	None	None	None	None	76.2μm**
Yoke Design				Revised	Revised
End Design	"yoke" set screws	"yoke" set screws	"yoke" set screws removed		

* Measures on conductor short samples

** 152.4 μm on diameter

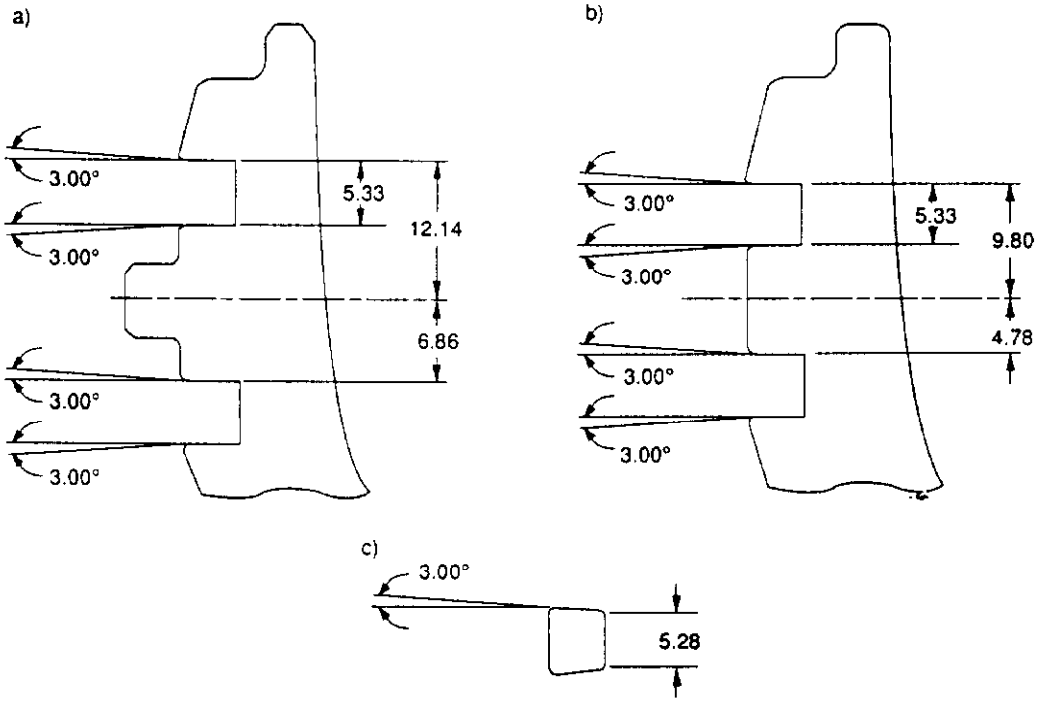

Figure 3. Collar key and keyway designs for most recent BNL 4-cm aperture, 17-m-long collider dipole prototypes: a) round collar keyway, b) anti-ovalized collar keyway, c) key (the key design is common to the two types of collars).

Collar-Yoke Interference

Tests on DC0201 suggested that the 254 μm reduction of the collar vertical diameter permitted the collared-coil assembly to loose contact with the yoke along the vertical axis in the cold state. Subsequent magnets therefore included brass shims of 76.2 μm each at both top and bottom of the collared-coil assembly. The shims were secured with double adhesive tape with a thickness of about 100 μm before compression and with a tested post-compression thickness of less than 25 μm.

Revised Yoke and Yoke Alignment Keys

The round collars used on magnets prior to DC0201 had horizontal tabs at the midplane which fitted into grooves punched in the yoke (see Figure 3). These tabs were removed from the anti-ovalized collars, and the notches at the midplane of the yoke were replaced by straight edges.

Another difference between the DD series and DC series magnets is the material of the yoke alignment key at the midplane of the yoke. The DD series magnets use low-carbon magnetic steel keys, while the DC series magnets use non-magnetic stainless-steel keys. This change was made following computer simulations that showed it would reduce the iron saturation effects at high field. The maximum change in the sextupole harmonic due to non-linear properties of iron is calculated to be less than 0.4 units in the entire range of operation

of the DC series magnets (it would be 1.2 units if the keys were magnetic).[18] It was calculated to be 0.7 units for the DD series magnets.

Yoke Set Screws

Magnets DD0026 and DD0027 included yoke set screws, that is, screws in addition to the coil set screws which push against the G10 shoe (see above, "End Parts"). The yoke screws were located at the periphery of the end plates and pushed directly against the yoke, possibly causing a bending of the end plate. This bending was thought to potentially decrease the efficiency of the coil set screws. The yoke screws were thus removed from DD0028 and excluded from later magnet designs.

Cross-Flow Cooling

All five magnets incorporated a cooling scheme which involves the circulation of helium between the various cooling passages in the magnet. At set intervals, helium is directed from the top yoke cooling passages to the coil cooling passage, and from the coil cooling passage to the bottom yoke cooling passages. This *cross-flow* of helium perpendicular to the magnet axis allows more of the total mass flow to participate in removing heat from the synchrotron radiation and maintaining the coil at a suitable temperature.[19] The scheme is realized by partially blocking the two top yoke cooling passages at one end, and the two others at the other end, thus creating a radial pressure difference which instigates the cross-flow; the cross-flow occurs at the stainless-steel laminations separating the yoke modules (see above, "Yoke and Shell"). In addition, helium must be prevented from leaking from the cross-flow path into spaces such as the loading flat between the collar and the yoke. Silicon (RTV) or indium plugs are thus periodically placed in these gaps to obstruct any such flow.

The blocking of the yoke cooling passages at the magnet ends is realized by inserting a plug into a stainless-steel tube mounted between each helium cooling passage of the last yoke module and the corresponding end-plate hole. On all five magnets, the stainless-steel tubes were tack-welded to the end plates and sealed with RTV into the yoke cooling passages as a safety precaution against high helium pressure during a magnet quench. Since then, it was thought that the RTV sealing might result in a rigid mechanical connection between the end plates and the yoke. The tubes were thus pushing against the yoke in a manner similar to that of the yoke set screws, which could produce a similar bending of the end plates. The mounting of the tubes was thus modified on the subsequent magnets of the DC series.

Instrumentation

All five magnets have the same standard instrumentation: voltage taps, strain-gauged collar packs, bullet gauge assemblies, and temperature sensors.

Voltage Taps

The total number of voltage taps is 41, all of which—except the quarter-coil voltage taps used for quench detection—are located on the inner layer of the coil. The instrumented turns are the three turns of the first block near the pole, and the first turn of the second block adjacent to the wedge. Extra taps are also located in the ramp-splice area where the inner conductor ramps up to the radius of the outer layer and is spliced to the outer layer conductor.

Strain-Gauged Collar Packs

Magnets DD0027 and DD0028 are equipped with two strain-gauged collar packs each; these are located at the minimum and maximum inner coil sizes. The packs each contain eight beam-type strain-gauge transducers to measure the azimuthal pressure exerted by the different quarter coils against the collar pole, as well as six compensating gauges, two for the inner layer transducers, and four for the outer ones.[11] The other magnets have only one strain-gauged collar pack, located at the minimum inner coil size.

Bullet Gauge Assemblies

All five magnets are also instrumented with special set screws at the turnaround end. These screws are machined to accommodate a small cylindrical piece, called the *bullet*, on which strain gauges are mounted to measure the force exerted by the coil against the end plate; these are designated as *bullet gauge assemblies*.[11] Each of the four bullets has two active gauges. The eight active gauges share two compensating gauges.

Temperature Sensors

The instrumentation of all five magnets also includes four carbon-glass resistor thermometers, two mounted in one of the four helium inlets in the lead-end end plate, and the other two mounted in one of the four helium outlets in the return-end end plate. These sensors were added to better track the coil temperature.

Test Stand Instrumentation

The test stands of the BNL and FNAL test facilities are equipped with instrumentation to monitor the flow of helium and other cryogenic parameters. In particular the stand instrumentation includes warm and cold pressure transducers at both ends of the magnet.

MAGNET ASSEMBLY

Coil Assembly

The four quarter coils are wound and cured separately, then joined during the assembly process.

Winding

The coils are wound onto convex, laminated mandrels using the *shuttle-type* winding machine pictured in Figure 4. The cable is fed from a quasi-static supply spool while the mandrel is shuttled back and forth longitudinally.[20] After the mandrel has travelled one length, the supply spool transfers to the other side of the mandrel, which in turn re-traces its path to complete one turn. The mandrel is also rocked azimuthally to ensure a proper lay of the cable, especially at the ends. Throughout the operation, the cable tension is maintained constant at about 175 N. For the outer coils, a 75 μm sheet of Teflon and fiberglass-impregnated tape are laid over the mandrel. This has been shown empirically to enhance the quality of the outer coil's inner surface which, in the final assembly, will rest against the inner coil.

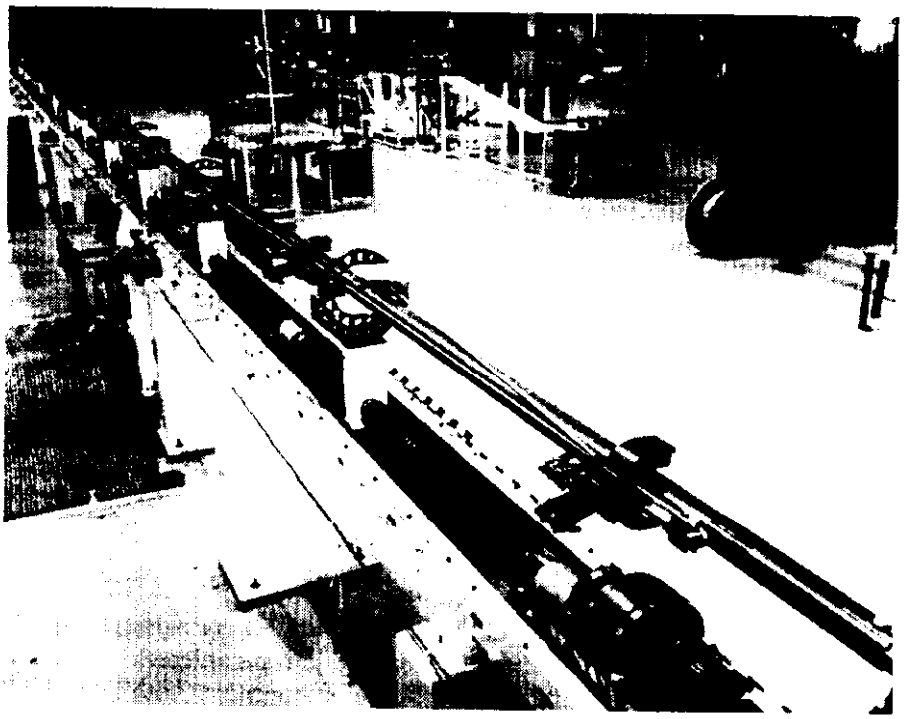

Figure 4. BNL shuttle-type winding machine for 4-cm aperture, 17-m-long collider dipole coils.

Curing

The objectives of curing are three-fold: 1) to polymerize the epoxy of the cable insulation, in order to make the coil rigid and thus easier to manipulate, 2) to form the coil into the correct shape and the correct dimensions, and 3) to make the coil as uniform as possible along the coil length. Correctness of the coil dimensions is important for the field quality. Uniformity of the coil is also required to achieve uniform pre-compression after collaring.

When winding is complete, the coil and mandrel are laid onto the bed of the curing press pictured in Figure 5. This bed consists of concave, laminated steel blocks, constructed to very accurate dimensions, and called the *form blocks*. These form blocks can be heated by the circulation of oil. Coil and form blocks are then covered by steel contact parts, called *top hats*, which are hydraulically pressed. The nominal curing pressure is 50 MPa ± 15 MPa for both inner and outer quarter-coils. The heating sequence includes several steps. The first phase consists in ramping up the temperature to 90° C, at which epoxy enters the gel phase. Measurements of the gaps between the form-blocks and the top hats are made along the curing fixture to determine the azimuthal size of the coil under the nominal curing pressure. These measurements are then used to determine the thickness of a shim to be inserted between the form blocks and the hat to bring the coil to a suitable size. The second phase is the curing itself, during which both temperature and pressure are increased, the former to 135° C, the latter until the gap closes between the form blocks and the top hats. These conditions are maintained for about 100 minutes. The last phase is simply cool down to room temperature. During the curing phase, the ends are also loaded to a nominal force of 8500 N.

Coil Size Measurements

When curing is complete, the coil is separated from its mandrel and placed on a stable fixture. A measuring device is then used manually to determine the azimuthal size of both sides of the coil along its straight sections. The measurement is taken at intervals of 0.75 m under a pressure of 70 MPa for the inner coil, and of 55 MPa for the outer coil. (These pressures are the target pre-compressions for the collaring.) Table 2 summarizes the coil size measurements for all five magnets. The values presented are the deviations between the actual measurements and the design values, averaged over the two inner and two outer quarter coils. It appears that the coil sizes vary slightly from magnet to magnet, presumably due to slightly different cable dimensions or slightly different curing conditions. However, it also appears that, for a given magnet, the standard deviation does not exceed 50 μm; the uniformity of the coils is thus very good. As we shall see later, the coil size measurements are used during collaring to achieve a suitable pre-compression. (Note that by measuring the coil size at different pressures in a given range one can determine the spring rate of the coil in that range. Measurements on the inner coils of the 4-cm-aperture, 17-m-long dipole prototypes lead to a spring rate of 0.2 MPa/μm in the range 35 to 80 MPa.)

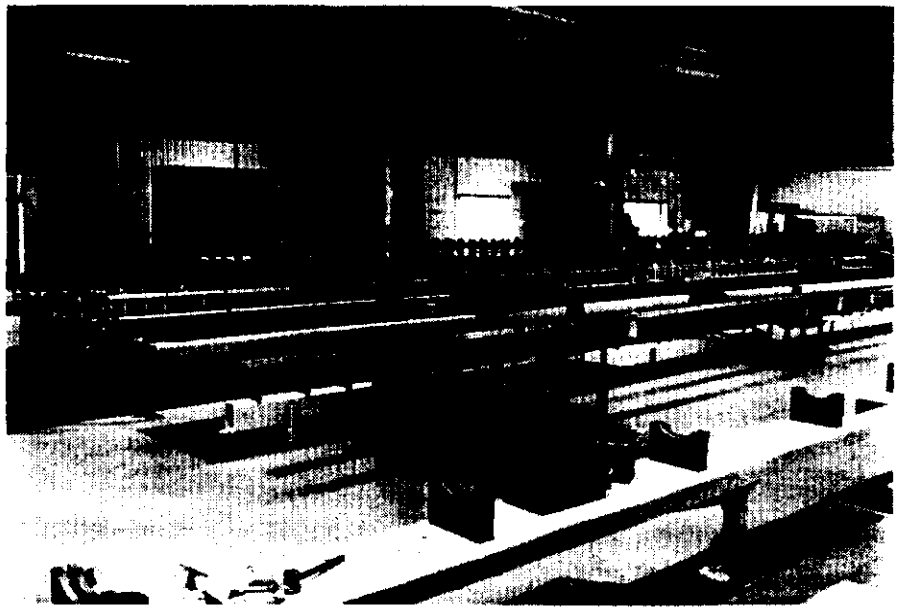

Figure 5. BNL curing press and molding fixtures for 4-cm aperture, 17-m-long collider dipole coils.

Table 2. Average Coil Size Deviations and Coil Shim Thicknesses of Most Recent BNL 4-cm Aperture, 17-m-Long Collider Dipole Prototypes (in μm).

Magnet Name	Inner Coil		Outer Coil	
	Size Deviation	Shim Thickness	Size Deviation	Shim Thickness
DD0026	122±49	640	−64±23	820
DD0027	138±51	640	−63±27	820
DD0028	61±27	640	−125±51	820
DC0201	−7±56	720	−162±39	770
DC0204	67±23	640	−74±23	720

Splicing and Final Assembly

In the final stages of the coil assembly, the four quarter-coils are first encased in Kapton caps to reinforce the ground insulation and reduce the risk of flashing between the edges of the conductor and the collars. The quarter-coils are then assembled into two coil halves, each consisting of one inner and one outer layer. A 50.8 μm sheet of Teflon is inserted between the two layers to smooth the interface. The layers of each half-coil are then connected electrically in series by what is called a *ramp-splice*.

The ramp-splice, represented in Figure 6, is formed as follows. First, conductor from the inner layer pole turn is bent radially in its plane in order to ramp up to the outer coil radius; bending begins 14 cm from the end of the inner coil straight section. The conductor is then spliced over a length of 76.2 mm to conductor from the outer layer pole turn using a 96% tin–4% silver solder. The ramp and splice are then encased in a G10 holder, 152.4 mm in length. For the DD series magnets, the area where the inner layer conductor enters the G10 holder was observed as the origin of a large number of quenches.[13] Therefore, starting with magnet DC0201, a length of conductor from the inner layer pole turn before the ramp was epoxied to the adjacent turn in order to prevent this turn from moving radially inward during collaring. (This is the only place on the coil where the turns are not laminated together.)

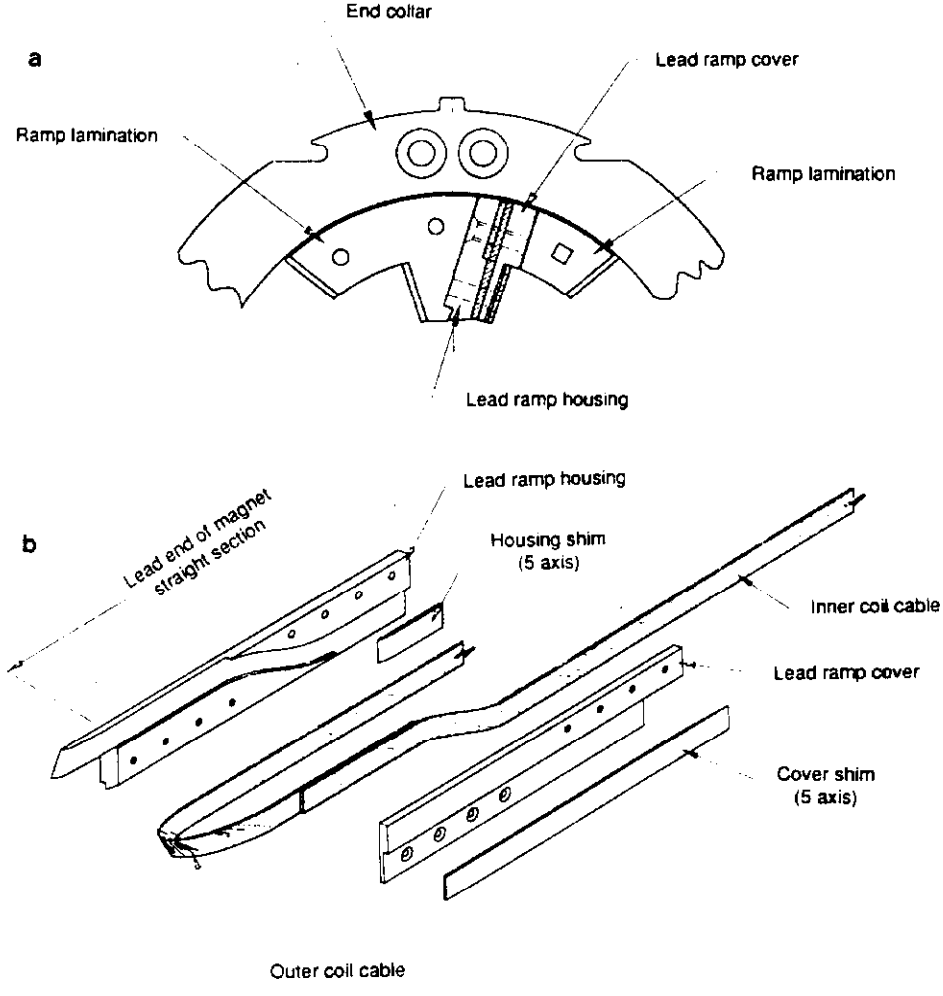

Figure 6. Detailed design of the Ramp Splice between the inner and outer layers of a BNL 4-cm aperture, 17-m-long Collider Dipole Coil: a) cross-sectional view, b) exploded view.

The coil halves, joined now via the ramp-splice, are then assembled around the beam tube, made of Nitronic 40 stainless-steel with a wall thickness of 127 μm. The outer surface of the coil assembly is covered by another teflon sheet (25 μm thick) and by several layers of Kapton, which complete the ground insulation and sandwich four copper-clad stainless-steel strip heaters (one per quadrant) for quench protection. The coil assembly is finally covered by a 381-mm-thick layer of stainless steel, called the *collaring shoe*, whose purpose is to protect the coil against the ripples of the collar laminations.

Collaring and Keying

Collaring is one of the most important steps in the magnet assembly. It is during collaring that the coil is pre-compressed, and it is this pre-compression which deflects the collars and creates the interference with the yoke along the vertical diameter. It is, therefore, crucial to achieving suitable pre-compression and suitable collar deflection in demonstrating the feasibility of the line-to-line fit design. Similarly, the design's feasibility hinges on whether the coil pre-compression and collar deflection for real magnets are reproducible enough to make these features part of a production process. We shall now describe the details of the collaring technique, and then discuss the reproducibility of the collaring data on our sample of magnets.

Pole Shim Optimization

Let s_m designate the measured azimuthal size of a given quarter coil under a pressure σ_m. The spring rate of the coil is a non-linear function of the coil stress; in the pressure range of interest (35 to 80 MPa), it can, however, be considered as constant.[21] The azimuthal coil size, s, can then be related to the coil stress, σ, and to the coil spring rate, k, by

$$\sigma = \sigma_m + k\,(s - s_m) \tag{1}$$

To achieve a target pre-compression, σ_0, the azimuthal size of the coil must be

$$s = s_m + \frac{\sigma_0 - \sigma_m}{k}\,. \tag{2}$$

The arc length, l, of the collar cavity containing a given coil layer must, therefore, be

$$l = s_u + s_l\,, \tag{3}$$

where s_u designates the azimuthal size of the upper quarter-coil of the given layer under the pressure σ_0, and s_l the azimuthal size of the lower quarter-coil. (In practice, s_u and s_l must be equal to avoid a skew quadrupole component in the magnetic field harmonics.)

The coil size and the coil spring rate depend on many parameters, including the conductor dimensions, the epoxy content of the insulation, and the curing parameters, which, in the course of an R&D program, are deliberately varied. To avoid stamping new collars for each magnet, it was, therefore, decided to design the collars with larger coil cavities than necessary and to introduce, between the collar poles and the coil, brass shims of adjustable thicknesses, referred to as *pole shims*. Let l_0 designate the fixed arc length of the collar cavity containing a given coil layer. The thickness, t, of the two identical shims to be inserted between the upper and bottom poles of the collar and the quarter-coils of the given layer is determined by

$$l_0 = s_u + s_l + 2t \ . \tag{4}$$

Now, the values of s_u and s_l to be introduced in Equation (4) must correspond to the target pre-compression σ_0. Since the coil properties can vary, the most reliable way to optimize the shim thickness is to measure the actual size under pressure of each individual quarter-coil before collaring, as described in the above section "Coil Size Measurements." Table 2 summarizes the coil size measurements of the magnets of interest. The values in Table 2 are, in fact, the differences between the actual coil sizes, s_m, and a design value, s_d, for the quarter coil of the given layer under a compression σ_m, which are then averaged over the upper and lower quarter coils. If t_d designates the design shim thickness, defined as

$$t_d = \frac{l_0}{2} - s_d \ , \tag{5}$$

the optimized shim thickness, t_o, is given by

$$t_o = t_d - (s_m - s_d) \tag{6}$$

(In deriving Equation (6), we assume that $\sigma_m = \sigma_0$. If it does not, the sizes would have to be corrected using Equation (2).)

Whereas in principle, it would be possible to take many coil size measurements and to custom design shims for each individual collar pack, this would considerably increase assembly time. Therefore, in practice, custom design shims are used only for the packs covering the coil ends or at the axial locations where there are large deviations in the coil sizes. For the straight sections, the optimization is done on average over the coil length, and an average shim thickness is calculated for each of the coil layers. Trials are then performed in order to verify the shim sizing in relation to the target pre-compressions. If the target pre-compressions are not achieved, the shim thicknesses are adjusted. Table 2 presents the result of this optimization for the coil straight sections of the magnets of interest. (The target pre-compression is 70 MPa for the inner layer and 55 MPa for the outer layer; the design shim thickness is 533.4 μm for the inner layer and 660.4 μm for the outer layer.) Shims of the pre-determined thicknesses and of the same length as the collar packs are then mounted on the eight faces of the collar poles of each pack. In order to avoid sliding during collaring, they are *mechanically seated* by means of small tabs fitting into grooves in the end of each pack.

As we mentioned earlier, these shims are used only during the R&D phase of the program. Once the parameters of the design are entirely determined and the fabrication process is under control, the thicknesses of the shims should no longer vary from magnet to magnet. It will then be a matter of correcting the pole angle of the collars to include this extra thickness (while keeping the sextupole harmonic of the magnetic field within specifications).

Collaring Process

Once the shims have been installed on the collar packs, the packs are placed manually around the coil and beam tube assembly, starting from the *lead end* of the coil, where the electrical connections are located. The assembly is then placed onto a precision, carefully aligned bed against which the collaring press operates. The press itself is about 2 m long and is moved along the collaring bed as pictured in Figure 7. It is equipped with two series of hydraulic cylinders. The vertical cylinders are used to press vertically on the top and bottom halves of the collar packs until the keyways at the collar sides are almost aligned. The

horizontal cylinders are then pressurized incrementally to drive the tapered keys into the keyways, as the vertical cylinder pressure is incrementally reduced. Once the keys are inserted, the horizontal pressure is released.

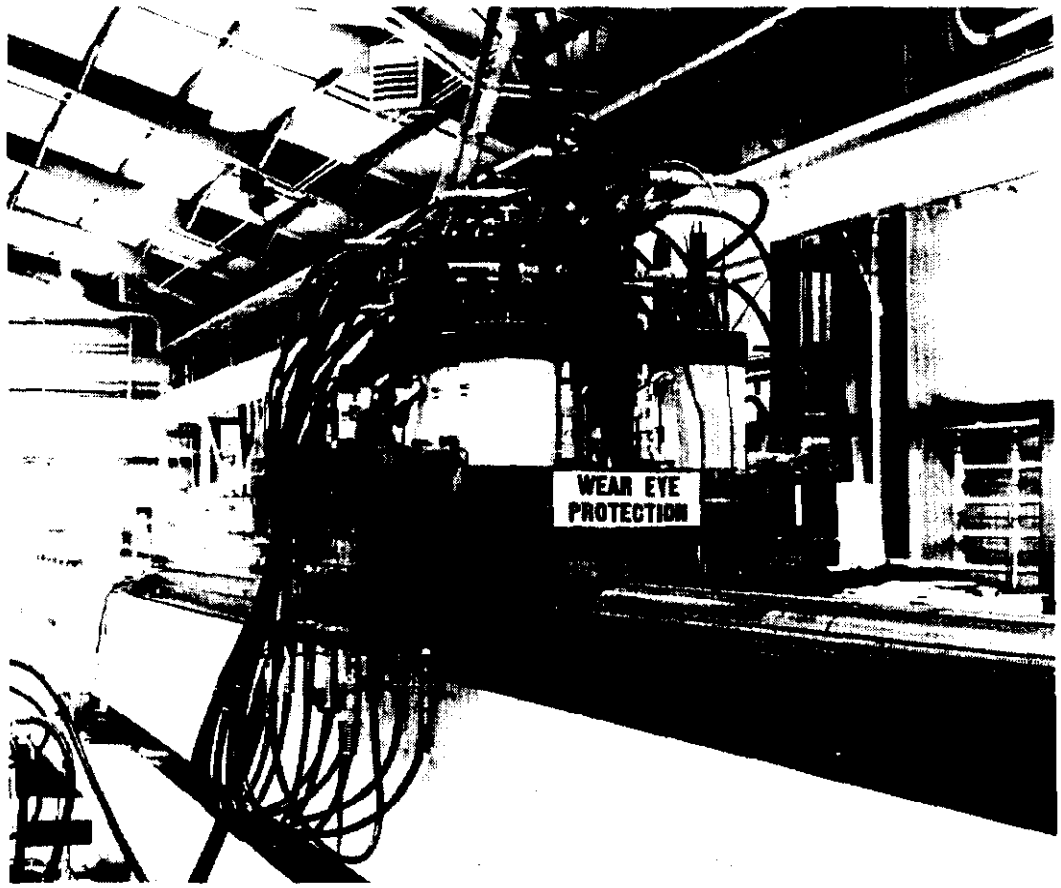

Figure 7. BNL collaring press for the 4-cm aperture, 17-m-long collider dipole prototypes.

Figure 8 shows typical profiles of the collaring pressures and of the pressure exerted by the coil against the collar pole during assembly, as measured by the beam-type strain-gauge transducers of the strain-gauged pack. The coil stresses presented here are averaged over the four transducers of each layer. As can be seen in Figure 8, coil compression increases as vertical pressure is applied. It is maintained roughly constant during key insertion, then jumps down as the collaring pressures are released. What we referred to earlier as target pre-compression is, of course, the pre-compression that remains once the collaring is completed. This level of pre-compression is achieved by appropriately sizing the pole shims; but to assemble the collared coil, the keys must be inserted, and, for a given shim size or, more generally speaking, *coil package* size, the key insertion requires that the coil be compressed to a higher level than that of the target pre-compression.

As mentioned in the introduction, the peak pressure during collaring must be limited because it creates a risk of damaging the coil insulation. This led to the use of tapered keys.[16]

The advantage of tapered keys over squared keys is that due to their taper they can be forced into the keyways without these being perfectly aligned. In the case of square keys both halves of the collar needed to be perfectly joined so that the keyways would be fully open before insertion of the keys. But in the case of tapered keys, part of the horizontal driving force can be used to fully open the keyways, and thus to complete the conjunction of the collar halves. Because the keyways need not be as open as for the squared keys, less vertical pressure is required to start the key insertion, which in turn allows one to limit the peak stress seen by the coil during collaring. In the case of 4-cm SSC dipole prototypes, the overpressure needed to insert square keys can be as high as 140 Mpa, while that to insert tapered keys can be limited to the desired 70 MPa.

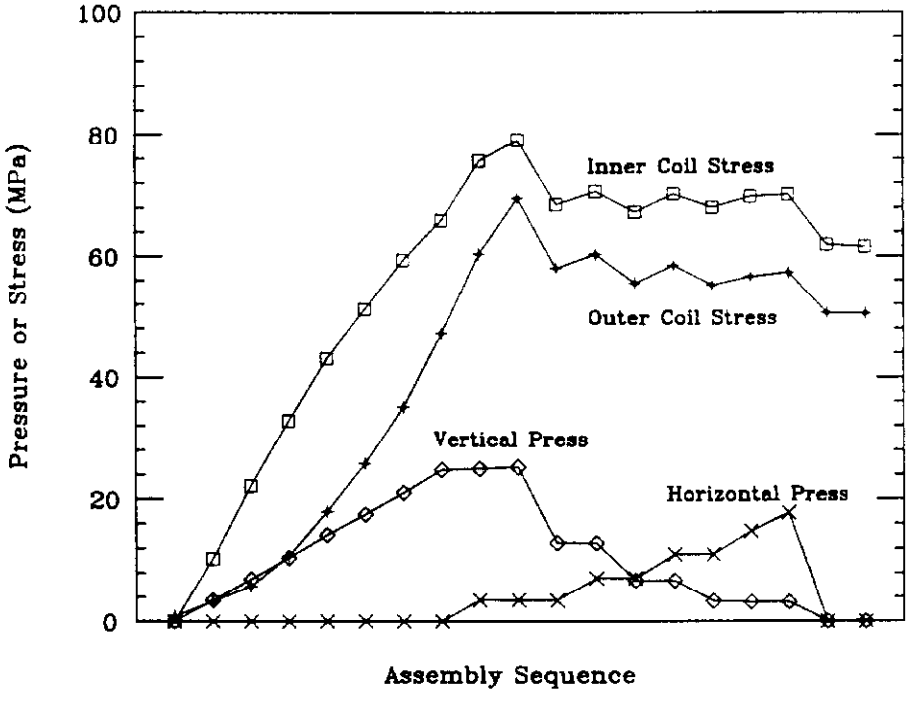

Figure 8. Collaring pressures and coil stresses during the collaring of BNL 4-cm-aperture, 17-m-long collider dipole magnet prototype DC0204.

Another advantage of the tapered key technique, which also goes in the same direction, is that it permits control of the *spring back* of the collars at the time of the collaring pressure release. This spring back comes from the fact that, while they are under the collaring press, the collar arms are in compression; after the completion of collaring and keying, the collar arms of the keyed assembly are in tension. At the time of the collaring pressure release, the collar arms thus spring back from compression to tension. This effect is particularly dramatic for the square key collars which are overcompressed to fully open the keyways. It can be greatly reduced (and even eliminated) in the case of tapered keys, which can be driven against the loading surface of the collar keyway, thereby pre-tensioning and elongating the collar arms (in the elastic range) as they end up in the keyed assembly. The spring back of square key collars is typically between 25 and 35 MPa, that of tapered key collars usually less than 15 MPa.

A feature of the tapered key insertion method is that as the keys load the collar keyways and complete the collar halves conjunction, they increase the clamping force on the

coil. The vertical collaring pressure can then be decreased accordingly to maintain a constant coil pressure during the operation. This is clearly illustrated in Figure 8, where, as the horizontal pressure is incrementally applied, the vertical pressure is incrementally reduced, and both inner and outer layer stresses stay constant. This also helps reduce coil overpressure during collaring. In practice, a film of lead-based lubricant is applied to the tapered keys to facilitate their insertion.

As we described, the primary reason for using tapered keys is to limit coil overpressure during collaring. On the other hand, the main objection to the tapered key technique is that as the keys are inserted and force open the keyways, they can distort the keyways or become distorted themselves. This can result in non-uniformities on the vertical diameter of the collared-coil assembly along the magnet length, and thus in magnetic field distortions. On the other hand, in the case of squared keys, the complete opening of the keyways is effected by the vertical pressure, and the keys could virtually be inserted by hand. Thus there is minimal key distortion and minimal risk of non-uniformity. Later, we shall see that although the tapered key technique on earlier prototypes led to somewhat erratic distortions,[22] it now seems under control. (Another disadvantage of the tapered key technique is that the horizontal force, used to drive the keys in, also loads the coil at the midplane, eventually causing the midplane turns to move inward.)[23]

Coil Compression Comparison

The target pre-compressions are 70 Mpa for the coil inner layer, and 55 MPa for the coil outer layer at room temperature. Having described the collaring process, we now need to verify that these targets can be reached and that the eventual fluctuations from magnet to magnet are not random.

To make cross-magnet comparisons, however, we need to find a sensible way to reduce the data. From what we described above, coil compression results from squeezing the coil into a cavity smaller than its size at rest. Fluctuations in the coil compression are, therefore, expected to originate from differences in the collar cavity sizes and in the size of the coil package itself (and eventually.in the coil modulus). Two types of collars were used for the magnets described in this paper: round and anti-ovalized. The anti-ovalized collars have the same geometry as the round collars, except that the location of one of the keyways has been displaced by a distance $2a = 254$ μm towards the midplane. Compared to that of the round collars, the arc length of the anti-ovalized collars cavity is, therefore, reduced by $2a$, for both inner and outer layers. On the other hand, the coil package size can be calculated by adding the shim thickness and the actual quarter-coil size. An appropriate parameter for cross-magnet comparisons seems to be the parameter m defined for each layer by

$$m = t + (s_m - s_d) \text{ for round collars, and} \tag{7a}$$

$$m = t + (s_m - s_d) + a \text{ for anti-ovalized collars.} \tag{7b}$$

In the following, we shall refer to m as the *effective size* of the coil package.

Figure 9(a) presents a plot of the inner coil stress, as measured by the beam-type strain-gauge transducers, versus the effective size of the inner coil package. The stresses reported here are the average stresses of the four strain-gauged pack transducers, and the value of m is calculated from the inner quarter-coil size measurements at the axial location of the strain-gauged pack. Squares mark the peak stress during collaring, and crosses mark the stresses just after collaring; diamonds represent data just before cool down, and circles

represent data just after cool down. (The data for the two strain-gauged packs of magnets DD0027 and DD0028 are differentiated by means of the letters LE and RE, referring to their locations with respect to the magnet ends: LE for the pack closest to the lead end, and RE for the pack closest to the other end of the magnet, also called the *return end*.) The main feature of Figure 9(a) is that at each step of the magnet assembly and after cool down, a linear correlation can be seen between the inner coil stress and the effective size of the inner coil package. Figure 9(b) presents the same kind of plot for the outer coil stress versus the effective size of the outer coil package. As in the case of the inner layer, linear correlations can be seen between the outer stress and the effective size of the outer coil package, although the data here are more dispersed. Two conclusions can be drawn from Figures 9(a) and 9(b): 1) a suitable collaring scheme can be developed to allow the coil to be pre-compressed to the desired level with a limited overpressure, and 2) the coil itself, despite its heterogeneities and the sensitivity of its parameters to the fabrication process, can be made to behave reproducibly. This is a first step in demonstrating the feasibility of the line-to-line fit design described in this paper.

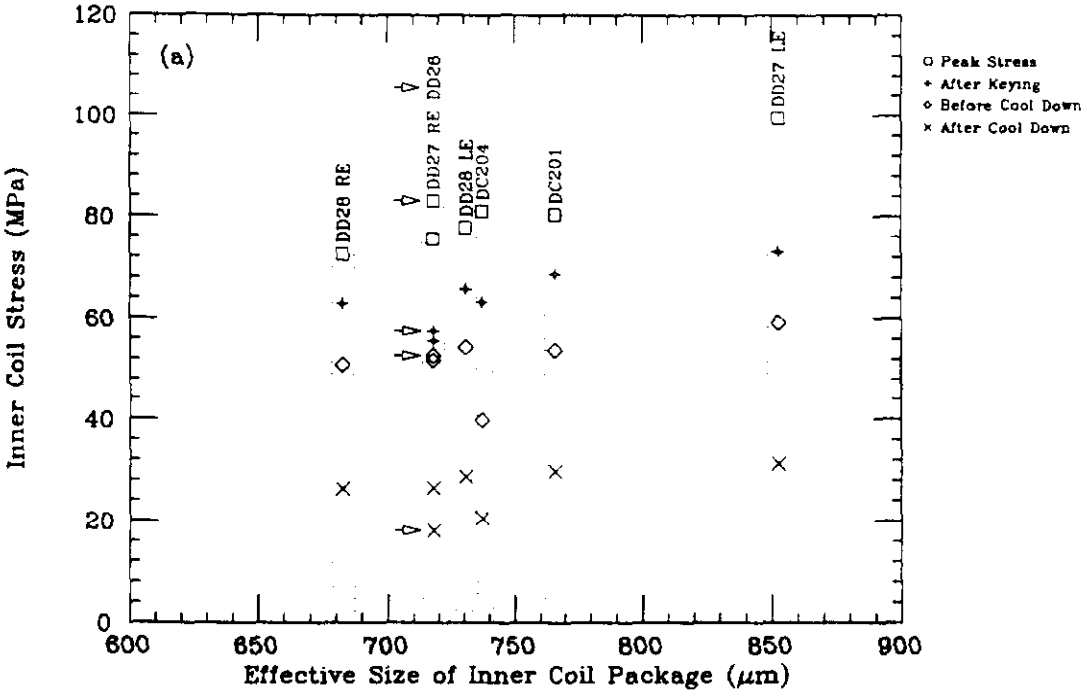

Figure 9(a). Summary of coil stresses at various times of assembly and testing versus effective sizes of coil package for most recent BNL 4-cm aperture, 17-m-long collider dipole prototypes: a) inner layer stress versus effective size of inner layer package.

An apparent spring rate can be calculated from the slope of the data on Figure 9(a) for each step of the magnet assembly and after cool down. For the data just after keying, the spring rate appears to be two-to-three times smaller than that measured on the quarter-coils prior to assembly: 0.08 compared to 0.2 MPa/μm. This discrepancy arises from the fact that the quarter-coil size measurements prior to assembly are done in a rigid cavity, while the apparent spring rate measured on Figure 9(a) results from the combination of three springs, the two coil layers and the collar arm, which can deflect radially. The spring rate decreases to about 0.05 MPa/μm for the data just before cool down and to 0.03 MPa/μm for the data just

after cool down. This apparent softening is concomitant with a decrease of the coil stress itself and presumably results from it, as the Young's modulus of a superconducting coil is not constant and tends to decrease with decreasing stress.[21] The reason the inner coil stress decreases by about 10 to 15 MPa during the few months that separate the time of keying and the time of testing has not yet been fully investigated and is probably due to creep in the insulation. (Note that this effect is not observed in the outer quarter-coils. This maybe related to the fact that only the inner quarter-coils see pressures above the yield point of Kapton.)

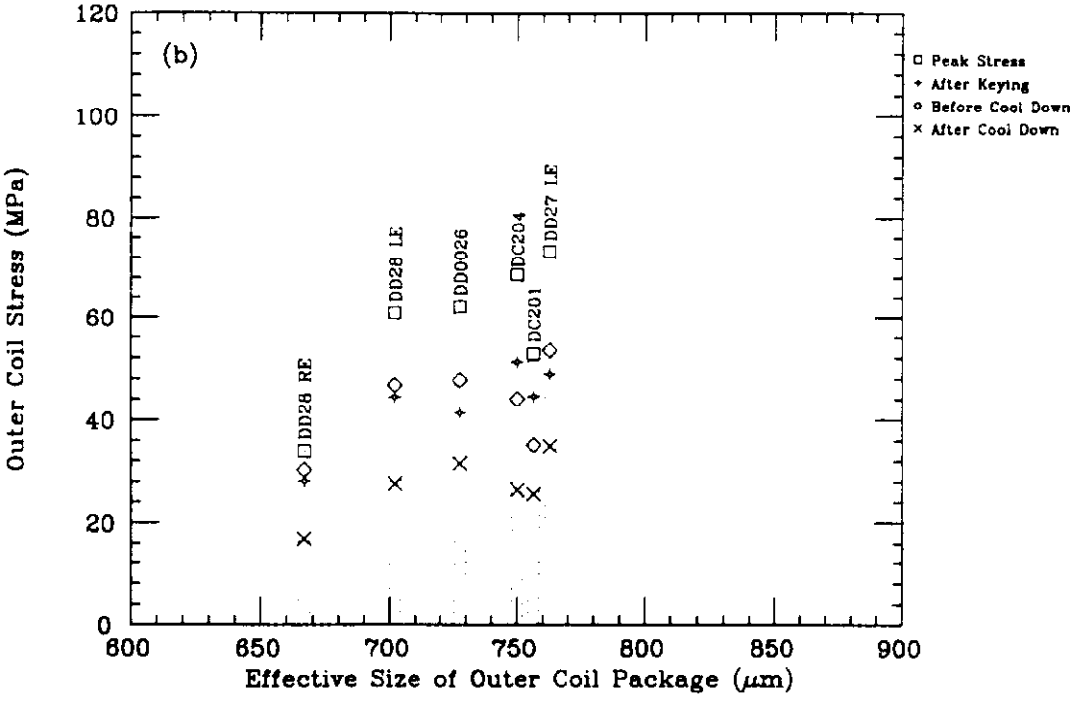

Figure 9(b) Summary of coil stresses at various times of assembly and testing versus effective sizes of coil package for most recent BNL 4-cm aperture, 17-m-long collider dipole prototypes: b) outer layer stress versus effective size of outer layer package.

Collar Deflection Comparison

Having established the feasibility of a suitable and reproducible level of coil pre-compression, it now remains to verify that this coil pre-compression results in suitable and reproducible collar deflections.

A nominal collar deflection along a given axis can simply be defined as the difference between the measured diameter of the collared-coil assembly along this axis and the design inner diameter of the yoke along the same axis. There is no problem in comparing horizontal deflections of round and anti-ovalized collar magnets, because they have the same horizontal dimensions. For the vertical deflections, however, there will be an offset of amplitude $2a$. For cross-magnet comparison purpose, we shall, therefore, use for the vertical deflection an effective deflection, d_{ve}, defined by

$$d_{ve} = \text{nominal vertical deflection for round collars,} \qquad (8a)$$

and

$$d_{ve} = \text{nominal vertical deflection} + 2a \text{ for anti-ovalized collars.} \qquad (8b)$$

Now, the collar deflections result from the simultaneous compression of the inner and outer coil layers. The relevant parameter to do cross-magnet comparison of these deflections is, therefore, the average stress, σ_a, defined by

$$\sigma_a = \frac{\sigma_i w_i + \sigma_o w_o}{w_i + w_o}, \qquad (9)$$

where σ_i and σ_o designate the inner and outer layer stress, and w_i and w_o designate the inner and outer conductor widths.

Figure 10 features a plot of the effective vertical deflection (upper data) and the nominal horizontal deflection (lower data) versus the average stress. (The deflections are that measured at the location of the strain gauge packs.) The main feature of figure 10 is that the collar deflections appear to be relatively independent of the average stress. This is certainly true for the vertical deflections which lie within 50 μm of each other. The horizontal deflections exhibit more dispersion, but this dispersion may be related to the fact that different magnets were keyed with different horizontal pressures.

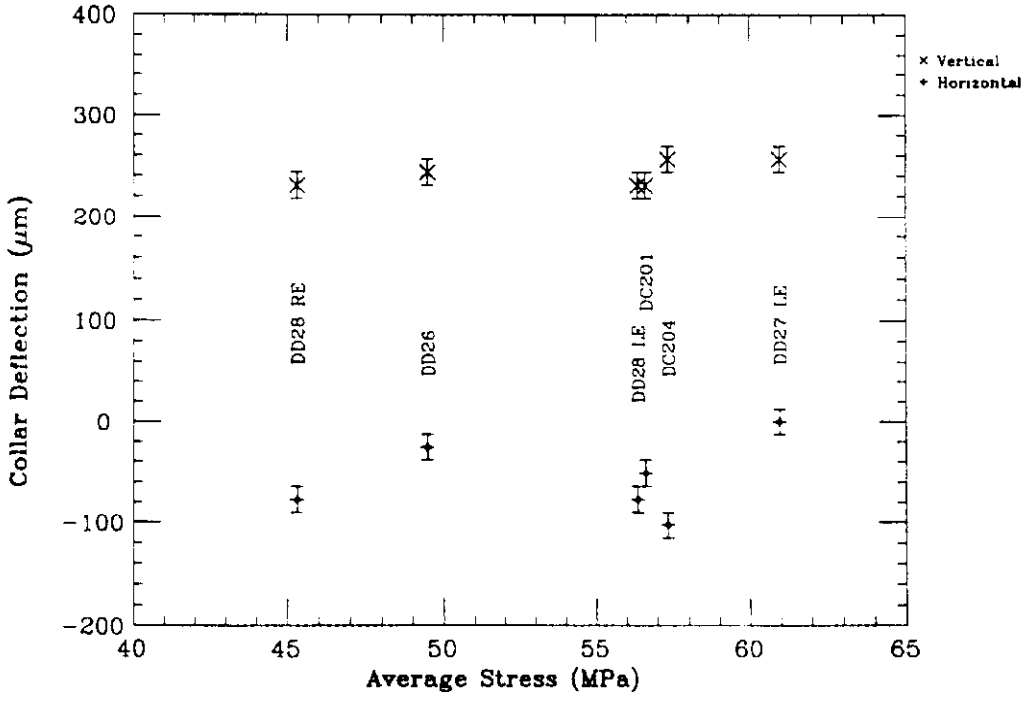

Figure 10. Summary of horizontal and vertical collar deflections versus average coil stress for most recent BNL 4-cm aperture, 17-m-long collider dipole prototypes.

The fact that the collar deflections do not relate to the average stress indicates that the deformations of the collared-coil assembly are inelastic. This inelasticity is probably introduced by scoring of the tapered key during the keying procedure described above. However, unlike the earlier prototypes where the scoring of the keys lead to erratic collar

deflections, [22] it now appears that the collared coil can be assembled in order to produce a consistent and suitable vertical deflection, with a limited, inward horizontal deflection. These inelastic deformations are therefore no longer thought to be a problem. They can even be seen as a advantage since, to some extent, they decouple the collar deflections from the azimuthal stress, thus rendering the shape of the collared-coil assembly less sensible to the mechanical properties of the coil. The reproducibility of the collar deflections demonstrated in figure 10 is a second step in demonstrating the feasibility of the line-to-fit design.

Yoke Stacking and Shell Welding

Yoke stacking and shell welding operations are straightforward. First, the bottom yoke halves are stacked and aligned on a precision plate. Alignment bars are inserted through the electrical bus slot, and tie rods are drawn through the yoke tube holes to hold the modules together (both the bars and the rods are removed at the end of shell welding). The bottom half shell is then assembled around the bottom yoke, and yoke and shell are rotated 180°. Next, the collared-coil assembly is laid into the bottom yoke halves and is covered with the top yoke halves and shell. The two shell halves are clamped with stainless-steel clamps, called *band clamps*. These are tightened until the gaps between the two shell halves on each side of the magnets are reduced to 1.5 mm. The two halves are then tack-welded every 30 cm, and the band clamps are removed. Last, the gaps between the shell halves are filled up by two successive welding passes, called the *root pass* and the *final pass*. Welding is done manually by two welders, one on either side of the cold mass, who try to stay in step with one another. The welding rod material is 308L stainless-steel.

As we described throughout the paper, the key idea of the line-to-line fit design is to assemble the collared coil so that it will interfere with the yoke on the vertical diameter. The first step in verifying that this interference occurs is to measure the collar deflections. The second step is to verify that a gap remains between the two yoke halves after they are placed around the collared coil assembly. On the other hand, as we also described earlier (see above, "Yoke and Shell"), a gap at the yoke midplane is undesirable in the cold state because it would alter the rigidity of the coil support against the radial component of the Lorentz force. A conservative solution to this problem is to ensure that the yoke gap is closed at room temperature by the end of shell welding. The closure of the yoke gap is thus monitored throughout the welding process through small openings of a few centimeters each, which are left every 2 m along the welding path, and where thickness gauges can be inserted.

Table 3 presents a summary of the yoke gap history during shell welding of some of the magnets described in this paper (the values are averaged over all measurements, on both sides of the cold mass). It can be seen that for the DD series magnets, which use round collars, a small gap remains after the shell welding. It is to correct for this gap that anti-ovalized collars were designed. Indeed, magnet DC0201, which was the first magnet to use anti-ovalized collars, shows no gap at the yoke midplane. In the case of DC0201, however, the gap appears to be closed from the beginning of assembly. This raises the question of whether there is an adequate yoke-collar interference on the vertical diameter. It is to resolve this uncertainty that shims were added at the top and bottom of the collared coil assemblies of the subsequent DC series magnets. The data for magnet DC0204 shows that the combination of anti-ovalized collars and collar-yoke shims produces the desired effect on the yoke midplane gap: it is wide open at the beginning of yoke assembly, ensuring the existence of a yoke-collar interference, and it is closed by the end of shell welding, dissipating worries about the coil radial support during energization. The yoke midplane gap can be controlled, and it can be verified during assembly that it is correctly open or closed. These two facts constitute another step in demonstrating the feasibility of the line-to-line fit design.

Table 3. Average Yoke Gap History During the Skinning of Most Recent BNL 4-cm Aperture, 17-m-Long Collider Dipole Prototypes (in μm).

Magnet	Pre-Tack	Tack	Root	Final
DD0027	270	140	90	50
DC0201	0	0	0	0
DC0204	250	160	90	0

End Plates

The last phase of the assembly is mounting of the end plates and setting of the screws, which load the coil ends axially. The first screws to be mounted are those of the return end, which contain the bullet gauge assemblies. The four set screws are tightened until the bullet gauges register a total end force of 4500 N. The torque value needed to reach this end force value is noted, so that the screws at the other end of the magnet, which do not contain bullet gauge assemblies, can be tightened to the same torque value. (The setting of the additional yoke set screws mounted on the end plates of magnet DD0027 was not recorded.)

Table 4 summarizes the total end forces measured by the bullet gauges at the end of the assembly of the magnets described in this paper. The numbers appear very consistent. Table 4 also lists the total end force registered by the bullets just before cool down of these magnets, after they have been mounted on the test stand. Although these measurements are also taken at room temperature and before any exercise of the magnets, the values appear widely spread and 2-to-3 times higher than they were at the end of assembly. The reason for this change has not yet been fully investigated, but it is probably related to shrinkage effects induced by the welding of the bonnet (see above, "End Parts") to the so called *single-phase bellows* of the test stand. (These bellows connect the magnet cold mass to the *end can* of the test stand for helium distribution.)

Table 4. Summary of Total End Force Measurements on Most Recent BNL 4-cm Aperture, 17-m-Long Collider Dipole Prototypes (in kN).

Magnet	Assembly	Before Cool Down	After 1st Cool Down
DD0026	4.55	8.25	4.35
DD0027	4.95	11.20	0.95
DD0028	4.60	15.05	8.10
DC0201	4.27	6.75	25.60
DC0204		8.55*	5.90

* One of the bullet gauges was discarded; the value is the average value over the three remaining gauges, times four.

CONCLUSION

In this paper, we reviewed the design features and fabrication processes of the five most recent BNL 4-cm-aperture, 17-m-long SSC dipole prototypes. For each step of the

fabrication (coil winding and curing, collaring, and yoke stacking and shell welding), we discussed the parameters that need to be controlled (coil sizes, coil stresses, and collar deflections, and yoke midplane gap), and compared their values for the five magnets. The data appear coherent and in line with the design concepts that were developed, demonstrating that the fabrication processes are under control. The next step will be to see whether these satisfactory assembly data translate into good quench performance and proper mechanical behavior at low temperatures. This discussion will be the object of a forthcoming paper.[6]

ACKNOWLEDGMENT

We are grateful to Jared Stark for his insightful comments on the manuscript.

REFERENCES

1. J. D. Jackson, ed., "Conceptual Design of the Superconducting Super Collider," SSC-SR-1020, March 1986; revised, September 1988.

2. J. R. Sanford and D. M. Matthews, ed., "Site-Specific Conceptual Design of the Superconducting Super Collider," SSCL-SR-1056, July 1990.

3. T. Garavaglia, K. Kaufman, and R. Stiening, "Application of the SSCTRK Numerical Simulation Program to the Evaluation of the SSC Magnet Aperture," SSCL-265, April 1990.

4. T. J. Peterson and P. O. Mazur, "A Cryogenic Test Stand for Full Length SSC Magnets with Superfluid Capability," *Supercollider 1*, M. McAshan, ed., 1989, pp. 551-559.

5. J. Strait, M. Bleadon, et al., "Fermilab R&D Test Facility for SSC Magnets," *Supercollider 1*, M. McAshan, ed., 1989, pp. 561-572.

6. A. Devred, T. Bush, et al., "Status of 4-cm Aperture, 17-m-Long SSC Collider Dipole Magnet R&D Program at BNL—Part II: Cold-Test Results," to be published.

7. J. Strait, B. C. Brown, et al., "Full Length Prototype SSC Dipole Test Results," *IEEE Trans. Magn.*, **23**, No. 2, March 1987, pp. 1208-1214.

8. J. Strait, B. C. Brown, et al., "Tests of Prototype SSC Magnets," *Proceedings of the 1987 IEEE Particle Accelerator Conference*, Washington, D.C., USA, March 16-19, 1987, pp. 1540-1542.

9. J. Strait, B. C. Brown, et al., "Tests of Prototype SSC Magnets," *IEEE Trans. Magn.*, **24**, No. 2, March 1988, pp. 730-733.

10. A. Devred, M. Chapman, et al., "Quench Start Localization in Full-Length SSC R&D Dipoles," *Supercollider 1*, M. McAshan, ed., 1989, pp. 73-83.

11. C. L. Goodzeit, M. D. Anerella, et al., "Measurement of Internal Forces in Superconducting Accelerator Magnets with Strain Gauge Transducers," *IEEE Trans. Magn.*, **25**, No. 2, 1989, pp. 1463-1468.

12. J. Strait, B. C. Brown, *et al.*, "Tests of Full Scale SSC R&D Dipole Magnets," *IEEE Trans. Magn.*, **25**, **No. 2**, 1989, pp. 1455–1458.

13. J. Tompkins, M. Chapman, *et al.*, "Performance of Full-Length SSC Model Dipoles: Results from 1988 Tests," *Supercollider 1*, M. McAshan, ed., 1989, pp. 33–49.

14. J. Strait, M. Bleadon, et al., "Full Length SSC R&D Dipole Magnet Test Results," *Proceedings of the 1989 IEEE Particle Accelerator Conference*, Chicago, IL, USA, March 20-23, 1989, pp. 530-532.

15. C. Goodzeit, P. Wanderer, et al., "Status Report on SSC Dipole R&D," to appear in the Proceedings of the 10th Workshop on the INFN Eloisatron Project —New Techniques for Future Accelerators, High Energy Intensity Storage Rings, States and Prospects for Superconducting Magnets, Erice, Italy, October 16-24, 1989.

16. C. Peters, K. Mirk, et al., "Use of Tapered Key Collars in Dipole Models for the SSC," IEEE Trans. Magn., **24**, No. 2, 1988, pp. 820-822.

17. A. K. Ghosh, M. Garber, et al., "Training in Test Samples of Superconducting Cables for Accelerator Magnets," IEEE Trans. Magn., **25**, No. 2, 1989, pp. 1831-1834.

18. R. Gupta, private communication.

19. R. P. Schutt and M. L. Rehak, "Transverse Cooling in SSC Magnets," Supercollider 1, M. McAshan, ed., 1990, pp. 209-217.

20. P. Dahl, J. Cottingham, et al., "Construction of Cold Mass Assembly for Full-Length Dipoles for the SSC Accelerator," IEEE Trans. Magn., **23**, No. 2, 1987, pp. 1215-1218.

21. T. Ogitsu, K. Maehata, et al., "Mechanical Hysteresis of Superconducting Coils," to be published.

22. J. B. Strait, private communication.

23. G. Spigo, private communication.